

See discussions, stats, and author profiles for this publication at: <https://www.researchgate.net/publication/311673014>

Prediction of Ship Manoeuvrability in Waves Based on RANS Simulations

Conference Paper · September 2016

CITATIONS

13

READS

638

2 authors:



Andrés Cura-Hochbaum
Technische Universität Berlin

25 PUBLICATIONS 317 CITATIONS

[SEE PROFILE](#)



Sebastian Uharek
FRIENDSHIP SYSTEMS AG

7 PUBLICATIONS 32 CITATIONS

[SEE PROFILE](#)

Prediction of Ship Manoeuvrability in Waves Based on RANS Simulations

Andrés Cura-Hochbaum and Sebastian Uharek
(Technical University Berlin)

Corresponding author, E-mail: cura@tu-berlin.de, Tel.: +49 30 314 24657

ABSTRACT

A novel numerical procedure for predicting rudder manoeuvres of a ship sailing in moderate regular waves is thoroughly described and validated with available experimental data. Only the mean effects of the waves are taken into account. The technique is purely based on RANS simulations of captive model tests in calm water and in waves and uses a mathematical model for determining the mean hydrodynamic forces and moments acting on the ship during the manoeuvres. The comparison of predicted and measured turning circle tests in regular waves show a very promising agreement.

INTRODUCTION

The permanent goal of reducing the installed power and exhaust gases of ships, along with IMO regulations regarding the Energy Efficiency Design Index (EEDI), has led to safety considerations with regard to minimum power requirements to ensure a reasonable manoeuvrability in waves. For this reason, the prediction of manoeuvring in waves has got more relevance in ship design and several research projects have started on this subject in recent years. The present paper describes a numerical prediction technique developed in the scope of the German project PerSee and the European project SHOPERA at the Technical University Berlin. In order to simulate rudder manoeuvres of a ship sailing in moderate seaways a mathematical model of Abkowitz type has been extended for taking mean wave forces and moments into account. This approach solely considers the mean effect of the waves, disregarding first order forces, which should not have a significant global influence on the resulting trajectories. This assumption seems reasonable as far as the encounter frequencies do not become excessively small, which can hardly occur when sailing in adverse conditions with small installed propulsion power and thus low forward speed.

OUTLINE OF NUMERICAL PROCEDURE

For manoeuvring prediction of displacement surface ships, it is usual to disregard dynamic changes of sinkage and trim during the manoeuvres. The motion equations of the ship, considered as a rigid body, result from the momentum and angular momentum equations. When written in four degrees of freedom in the hybrid Cartesian coordinate system that follows the ship motions, excepting roll, they read:

$$\begin{aligned} m [\dot{u} - \psi v - x_G \dot{\psi}^2 + z_G (2\dot{\psi}\dot{\varphi} \cos \varphi + \ddot{\psi} \sin \varphi)] &= X \\ m [\dot{v} + \dot{\psi} u + x_G \ddot{\psi} + z_G ((\dot{\psi}^2 + \dot{\varphi}^2) \sin \varphi - \ddot{\varphi} \cos \varphi)] &= Y \\ I_{xx} \ddot{\varphi} - I_{xz} \ddot{\psi} \cos \varphi + (I_{zz} - I_{yy}) \dot{\psi}^2 \sin \varphi \cos \varphi + \\ &\quad - m z_G \cos \varphi (\dot{v} + u \dot{\psi}) = K \\ (I_{yy} \sin^2 \varphi + I_{zz} \cos^2 \varphi) \ddot{\psi} + \\ 2(I_{yy} - I_{zz}) \dot{\psi} \dot{\varphi} \sin \varphi \cos \varphi - I_{xz} (\ddot{\varphi} \cos \varphi - \dot{\varphi}^2 \sin \varphi) + \\ m x_G (\dot{v} + u \dot{\psi}) + m z_G \sin \varphi (\dot{u} - v \dot{\psi}) &= N \end{aligned} \quad (1)$$

The velocity components of the ship's origin along the (horizontal) x- and y-axes are denoted by u and v , whereas ψ and φ are the heading and roll angles. The mass of the ship is m and the known coordinates of the centre of mass and moments of inertia referred to the ship fixed coordinate system are denoted by x_G , z_G , I_{xx} , I_{yy} , I_{zz} and I_{xz} . The ship has been assumed to be symmetric regarding $y = 0$, see Figure 1. Note that in practice we often assume $I_{yy} = I_{zz}$ and $I_{xz} = 0$ for simplicity, and thus the third and fourth equation become more compact.

Of course, heave and pitch can be significant in waves and in fact they lead to additional inertial terms disregarded in Equation 1 but we recall that we are going to include the mean wave effects only, and the corresponding mean inertial contributions will be contained there, see below.

The right hand sides in Equation 1 are the longitudinal and (horizontal) transverse force components (X, Y) and the longitudinal and (vertical) transverse moment components (K, N) along the axes of the hybrid system. Knowing the hydrodynamic forces and moments acting on the ship, it is straightforward to integrate these coupled differential equations numerically in time in order to simulate manoeuvres.

According to the idea mentioned above, we split the forces and moments in a component stemming from calm water and a component stemming from the waves:

$$\begin{aligned} X &= X_c + X_w \\ Y &= Y_c + Y_w \\ K &= K_c + K_w \\ N &= N_c + N_w \end{aligned} \quad (2)$$

The calm water part of the forces acting on the ship can be modelled with usual hydrodynamic coefficients, which can be determined by means of virtual PMM tests as explained in Cura Hochbaum (2006) and will be shown below.

Since only the mean effect of the waves on the manoeuvres is going to be taken into account, the corresponding part of the forces (and moments) represents the time averaged values of the second order forces acting on the ship for the considered “quasi-static” situation consisting of a given encounter angle α , wave length λ and forward speed u , see Figure 1. Thus, besides the limitation of the proposed procedure regarding the encounter frequency (or period) made above, there is an additional restriction regarding rapid heading changes. If the vessel is sailing with moderate yaw rates, which implies slow changes in the encounter angle α with a given single long crested wave, the vessel will experience several encounters with the “same wave” at each heading during the manoeuvre and the idealisation is expected to be reasonable.

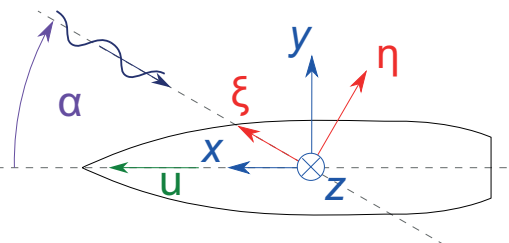


Figure 1: Coordinate system and wave direction.

Note that the procedure can be used for sea-ways as well, superposing the loads due to the individual wave components according to a given energy spectrum, see Faltinsen (1990). The mean values of the forces due to a single wave of given length and direction are obtained from RANS simulations as shown in the corresponding section below.

After the mean wave forces are obtained, their dependence on wave length and encounter angle can be modelled. This procedure has been described in Uharek and Cura-Hochbaum (2015). Due to the periodic behaviour of the mean force traces (mirrored at 180°) in the encounter angle, a Fourier series expansion is used to approximate this functional relationship. By assuming that the Fourier coefficients depend on the non-dimensional wave length $\lambda' = \lambda / L_{pp}$ and making a polynomial approach for these coefficients, the functional dependence on the wave length is captured as well:

$$F' = \frac{a_0}{2} + \sum_{n=1}^6 [a_n(\lambda') \cos(n\alpha) + b_n(\lambda') \sin(n\alpha)]$$

with $a_n(\lambda') = \sum_{i=0}^3 a_{ni} (\lambda')^i$ and $b_n(\lambda') = \sum_{i=0}^3 b_{ni} (\lambda')^i$

$$(3)$$

The force F' in Equation 3 denotes either X_w , Y_w , N_w or K_w of Equation 2, made non-dimensional with $(\rho g \zeta_w^2 L_{pp})$ or $(\rho g \zeta_w^2 L_{pp}^2)$, ρ being the water density, ζ_w the wave amplitude and L_{pp} the ship length. Note that according to Figure 1, $\alpha = 180^\circ - \mu$, being μ the usual encounter angle.

Since all forces have been divided by the squared wave amplitude, the non-dimensional forces can be considered independent of the wave amplitude as long as it does not become too large. The quantification of the valid range needs further research. In case of a low approach speed, the absolute speed loss during a manoeuvre is small, leading to a rather moderate influence of the forward speed on the mean wave forces. For higher approach speeds, the dependence of the mean forces on speed can be captured by generating coefficient sets at various speeds and interpolating the forces.

The numerical simulations needed for determining all hydrodynamic coefficients mentioned above, those corresponding to calm water as well as to waves, are performed with an updated version of the RANS code Neptuno, Cura Hochbaum and Vogt (2002). The code uses a finite volume method to solve the governing equations on a ship fixed, block-structured grid with non-matching interfaces. Pres-

sure and velocities are coupled by means of the SIMPLE algorithm (Patankar and Spalding (1972)) and the turbulence is modelled with the standard $k-\omega$ model from Wilcox (1993). The free surface is captured using a two-phase level set method, see Osher and Sethian (1988) and Sussman et al. (1994). A body force model is used instead of the propeller during the virtual captive tests. Hereby a force distribution in a certain region of the grid does approximate the effect of the (disregarded) propeller on the flow, depending on the current velocities at the propeller plane, see below. Contrary to Equation 1, ship motions are predicted with Neptuno by solving the motion equations in six degrees of freedom (without simplifications) together with the RANS equations.

In the following sections, the individual components of the prediction method will be described in more detail for the concrete case of the DTC, a very large single screw container ship, and the procedure will be used to predict manoeuvres in regular waves from different directions. The main dimensions of the DTC are shown in Table 1. The results are compared with ship model tests performed at the experimental facilities of MARINTEK.

Table 1: Main dimensions of DTC

	full scale	model scale
L_{pp}	355 m	3.98 m
B_{wl}	51 m	0.57 m
T	14.5 m	0.16 m
∇	173467 m ³	0.2452 m ³
c_B	0.66	
U	6 kn	0.327 m/s
GM	5.1 m	0.057 m
Fr		0.052
Re	$1.1 \cdot 10^9$	$1.3 \cdot 10^6$

DERIVATIVES FOR CALM WATER

In order to determine a complete set of manoeuvring derivatives for calm water for the DTC, virtual captive model tests have been performed at model scale.

Since the approach speed for all measured manoeuvres was chosen at a rather low speed of 6 knots, it was decided to simulate the virtual tests to determine the calm water coefficients without taking the water free surface and related effects into account. The grid was built using the commercial software GridPro and has a cylindrical zone with equal

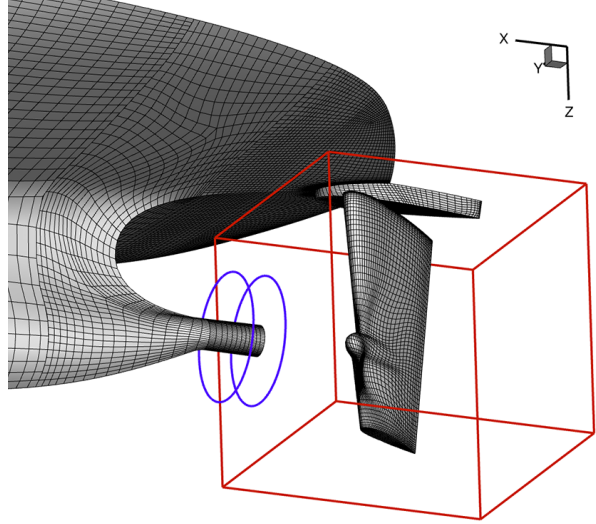


Figure 2: Grid for computations in calm water.

cell distribution for including the body forces in the propeller region, highlighted with blue lines in Figure 2, and a rudder box, indicated in red. For each considered rudder angle, a particular grid was generated within this box and included in the global grid using non-matching interfaces.

The test matrix for all virtual static tests is shown in Table 2. At first, some computations were performed to determine the propeller revolution rate at model self propulsion point (MSPP). The propeller revolution was then kept constant during all virtual tests. Since the DTC has a twisted rudder with a costa bulb, an asymmetric behaviour was expected. All rudder deflection tests were therefore performed to port and starboard up to 35° . This results in 11 tests for the straight ahead motion. These 11 rudder angle tests were performed for three additional drift angles ($\beta = -10^\circ, 10^\circ, 20^\circ$), three additional yaw rates ($r' = rL/u = -0.35, 0.35, 0.7$) and three additional forward speeds (-50%, -25% and +25%), resulting in a total number of 110 static tests. Due to the large metacentric height (GM), no tests in heeled condition were necessary in the present case.

Table 2: Matrix for virtual static PMM tests

rudder angle		11
drift / rudder angle	3 x 11	33
yaw rate / rudder angle	3 x 11	33
surge speed	3 x 11	33
total		110

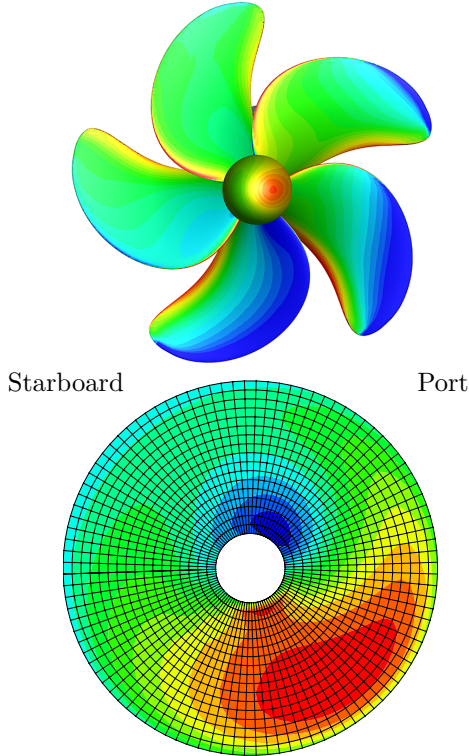


Figure 3: Pressure distribution on the blades and axial body force distribution on the propeller disk.

In addition to the static tests, five dynamic tests were computed mainly to determine hydrodynamic coefficients depending on accelerations, i.e. added masses and moments of inertia. Due to the small longitudinal speed, the motion period was chosen to 50s to avoid memory effects during the harmonic virtual tests. The computed tests were: one pure surge test with a non-dimensional amplitude of $\hat{u}' = \hat{u}/u_0 = 0.2$, one pure sway test with $\hat{v}' = \hat{v}/u_0 = 0.5$, one pure yaw test with $\hat{r}' = \hat{r}L/u_0 = 0.7$ and two combined sway/yaw tests with $\hat{v}' = -0.4, \hat{r}' = 0.7$ and $\hat{v}' = 0.4, \hat{r}' = 0.4$.

Especially for forces due to rudder deflection, it is important to take the propeller effect on the flow into account. This effect is approximated with a new developed body force model based on RANS simulations of 'oblique open water tests' for the considered propeller at different angles of incidence computed in advance.

As explained in Cura Hochbaum et al. (2016), the calculated pressures and shear stresses on the blades of the propeller for each given advance ratio and angle of incidence are transferred onto the propeller disk and averaged over one propeller revolution. Figure 3 shows a snapshot of the pressure

distribution on the blades of the DTC propeller in uniform flow at an incidence angle of 30° (from port side) and advance ratio 0.7 and the corresponding averaged axial force per unit area on the propeller disk. The blue regions at the propeller blades correspond to low pressures on the suction side and to high axial forces on the disk in red. The computations have been performed using the open source toolbox OpenFOAM.

The axial and transverse forces per unit area in each point of the polar mesh on the propeller disk are stored in a database for several advance ratios and incidence angles. This is used later on to determine the body forces in the propeller region during the RANS simulations of captive tests, depending on the current inflow to the propeller plane.

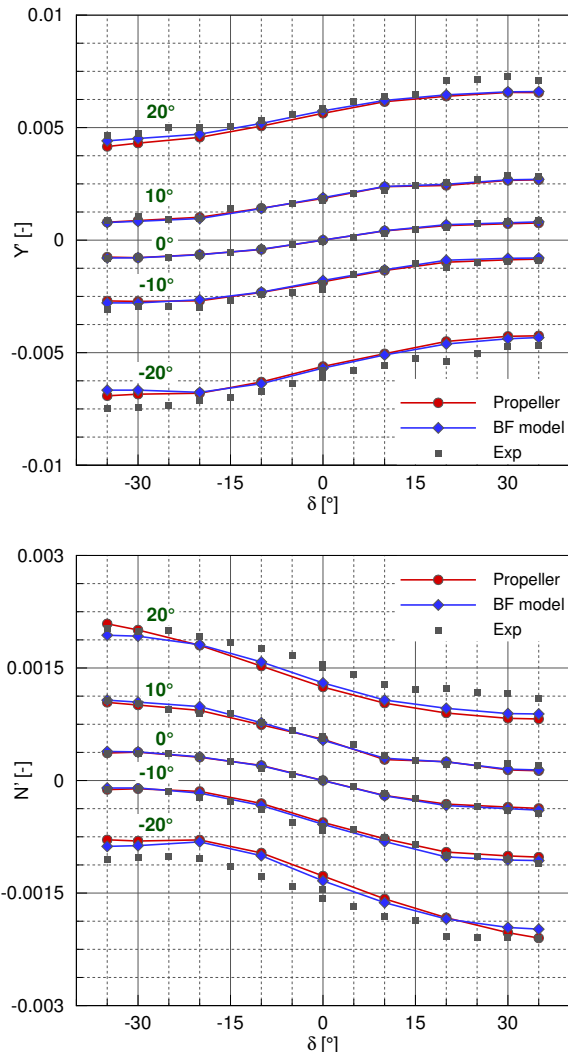


Figure 4: Side force and yaw moment determined with real propeller, body forces and experiments.

The accuracy of the body force model is surprisingly good. The model has proven to yield a very satisfactory agreement with experiments when applied for the propeller in behind condition during virtual manoeuvring tests. Figure 4 shows the non-dimensional side force and yaw moment on a medium size container ship in oblique towing condition at drift angles ranging from -20° to 20° combined with diverse rudder angles. The results using the present body force (BF) model are compared with those obtained by Yao (2015) considering the real propeller and with experiments from HSVA. There is almost no difference between them. Further, the calculated forces and moments agree reasonably well with measurements for all drift and rudder angles. At least for determining coefficients for manoeuvring prediction, it does not seem to be worthwhile to take into account the rotating propeller, which would be extremely time consuming.

Some interesting flow details from the virtual tests can be observed in the following two figures. Figure 5 shows the flow separation at the rudder, deflected to $\delta = -35^\circ$, during a rudder angle test at straight ahead condition. The horizontal cut plane is coloured with the axial velocity, blue corresponding to high values. The separation zone at the rudder and the propeller effect on the flow are clearly visible. The propeller disk has been coloured with the axial body force distribution and the rudder with the calculated pressure distribution, red corresponding to high values in this case. Figure 6 shows the velocity distribution in the propeller plane during an oblique towing or static drift test with $\beta = 20^\circ$. The flow is strongly accelerated and rotated by the body force distribution. The interaction between the “propeller” and the vortex on the leeward side (right hand side) can clearly be seen.

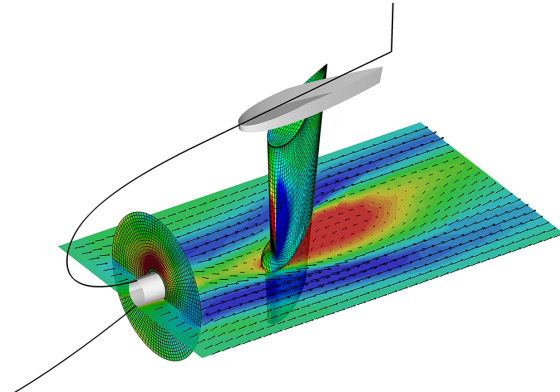


Figure 5: Pressure on rudder, velocity in a cut plane and axial body force on propeller disk.

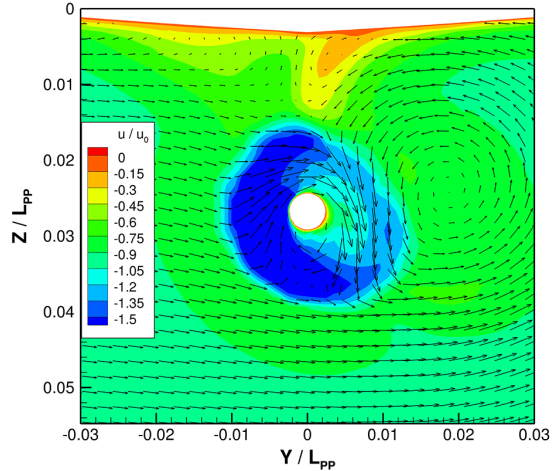


Figure 6: Velocity distribution in the propeller plane in steady oblique motion with $\beta = 20^\circ$.

In order to check the uncertainty of the computational results, selected cases have been calculated on grids of different resolution, ranging from 1.1 to 2.5 million cells, as shown in Figure 7 for the rudder. As in previous cases, the grid convergence behaviour has shown to be quite satisfactory. Figure 8 shows the resulting forces and yaw moment on three grids for the DTC in forced straight ahead motion with rudder deflected 35° to port. Note that not only the changes between grids are getting smaller, but that the largest difference between results on the coarse and the fine grid is smaller than 5%.

In addition, some of the calculations for determining rudder angle depending hydrodynamic coefficients and some drift angle dependent forces have been repeated with another RANS code, a customized solver for determining hydrodynamic coefficients using the open source toolbox OpenFOAM. Both codes were run on the same structured grid. Figure 9 and Figure 10 compare the computed non-dimensional forces and the yaw moment. Disregarding X' , the general agreement is very satisfactory.

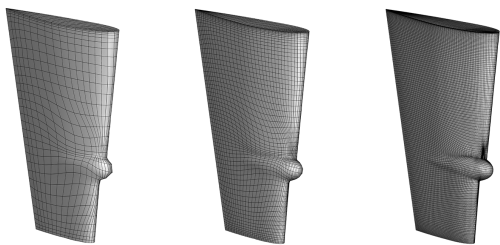


Figure 7: Different surface grids on the rudder

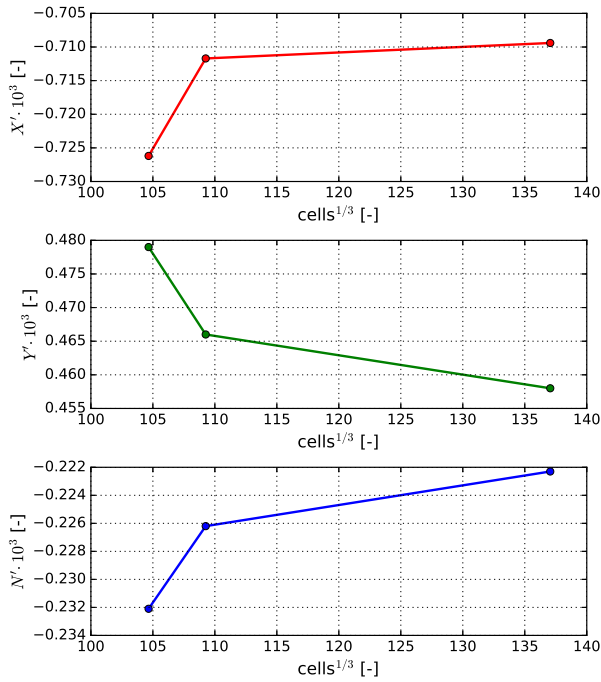


Figure 8: Dependence of calculated global forces and yaw moment on grid resolution.

The offset of the axial forces obtained with OpenFOAM simulations (green) in Figure 9 is explained by the fact that these have not been performed for exactly the same propeller revolutions corresponding to the self propulsion point. The grey traces, obtained without considering the propeller effect (w/o BF), show the very strong influence of the body forces on the predicted forces. The larger discrepancies of X' for different drift angles using OpenFOAM (green) and Neptuno (blue) in Figure 10 are most probably due to the different turbulence models used, $k-\omega$ SST and standard $k-\omega$, respectively. Additional static drift computations performed with OpenFOAM using the $k-\omega$ model yielded the red trace for X' in Figure 10, which is much closer to the one obtained with Neptuno, although the wall functions are different in both codes.

The hydrodynamic coefficients depending exclusively on motion parameters are determined by Fourier analysis of the dynamic tests. Rudder angle dependent coefficients are determined by multilinear regression of the forces obtained from the static virtual tests shown in Table 2. The lines in Figure 11 show the reconstruction of the non-dimensional global side force and yaw moment for all combinations of yaw rate and rudder angle using these

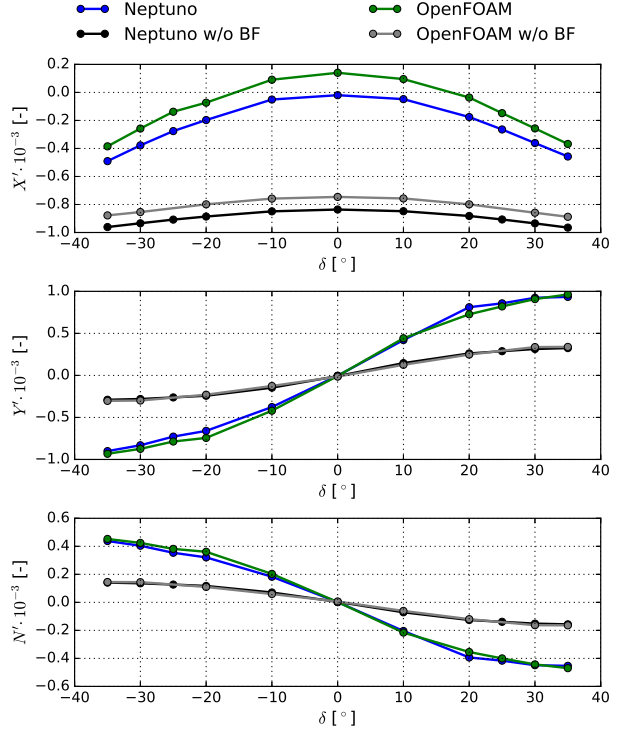


Figure 9: Rudder dependent forces computed with and without propeller effect and two RANS codes.

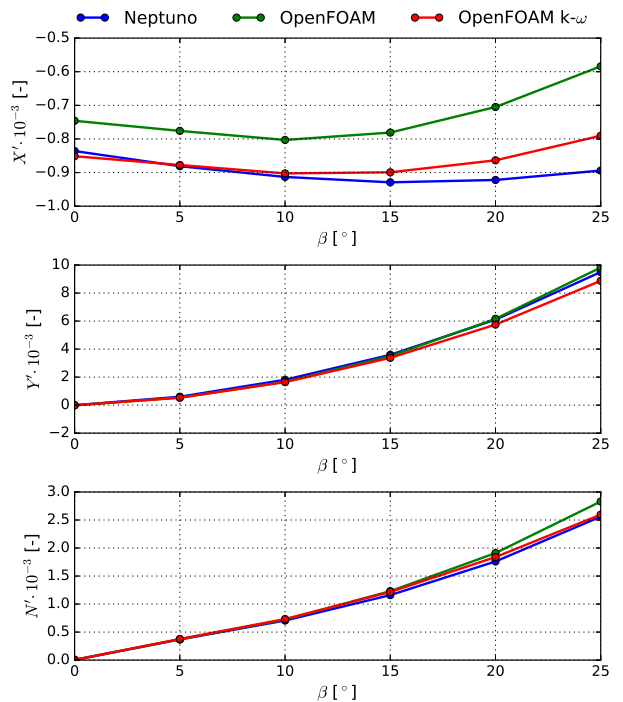


Figure 10: Drift angle dependent forces computed with two RANS codes.

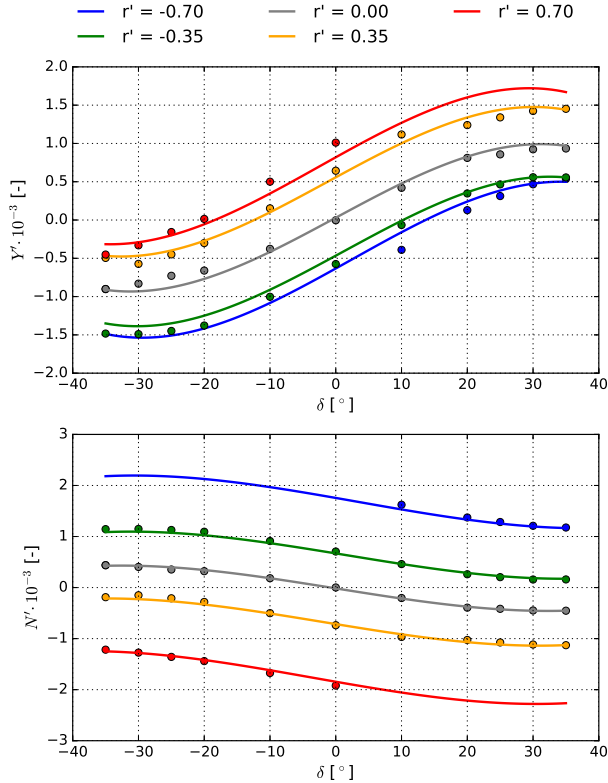


Figure 11: Calculated (symbols) and modelled (lines) side force and yaw moment.

coefficients. As can be seen, the rather simple mathematical model used, with coefficients up to third order, is able to predict the values in all situations quite well.

All computations are performed on a single core using a grid with 1.3 million cells. The average computation time for the static cases was 13.5 hrs. Due to the very large number of cases to be computed, there is no disadvantage in using a scalar RANS code. All computations can be performed simultaneously overnight on a PC cluster of a few hundred cores. The dynamic cases were computed using 10 SIMPLE iterations and 2500 time steps per motion period. The computation time was 60 hrs per motion period.

The basic model for calm water, consisting of hydrodynamic coefficients, which reflect the influence of all motion and steering parameters on the hydrodynamic forces and moments acting on the ship, has proven to perform satisfactorily for several applications as shown in the SIMMAN workshops, see Cura Hochbaum et al. (2008) and Cura Hochbaum and Uharek (2014).

MEAN WAVE FORCES

For the computation of wave forces acting on the hull, a new grid including the free surface has been created. Since the free surface is moving relative to the heaving and pitching ship, a spreading of the cells in the vertical direction at the inlet and outlet of the computational domain is necessary for an adequate resolution of the free surface. Figure 12 shows a slice at the centre plane of the ship. The red lines show the position of the free surface for pitch angles $\theta = \pm 1^\circ$.

All waves are computed on the same grid, thus the resolution was chosen sufficiently high as to ensure a good quality even for the smallest wave with non-dimensional length and amplitude $\lambda' = 0.3$ and $\zeta' = \zeta/L_{pp} = 0.004$. The resolution on the finest grid was 23 to 80 cells per wave length in longitudinal direction and 5 to 10 cells per wave height in vertical direction, depending on the wave considered. The domain extends $1 L_{pp}$ towards inlet and port side and $2.5 L_{pp}$ towards outlet and starboard side. The waves are generated at the boundaries in front and at the port side of the ship. To damp reflections at the opposite side and outlet the grid was expanded and additional damping terms have been added to the right hand sides of the RANS equations as well.

Figure 13 shows the quality check for a head quartering wave from port side with $\lambda' = 0.75$, $\alpha = 45^\circ$ and $\zeta' = 0.0075$. The blue trace shows the free surface elevation along a longitudinal vertical cut at the side of the ship $0.65L_{pp}$ towards the incoming waves, where the wave elevation is expected to be undisturbed at an early point of the simulation. The black dashed trace represents the Airy theory. As can be seen, the loss of wave amplitude is quite small in this case and the wave length is predicted very accurately in the range of interest $-0.5 < x/L_{pp} < 0.5$. Far behind the ship, the grid expansion leads to a (desired) considerable wave damping.

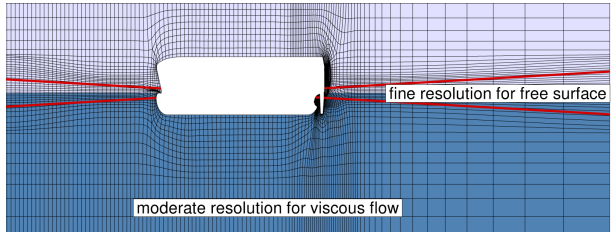


Figure 12: Spreading of the computational grid to account for pitch motion in waves.

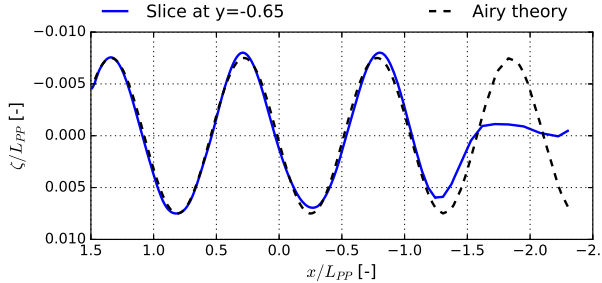


Figure 13: Computed and theoretical wave.

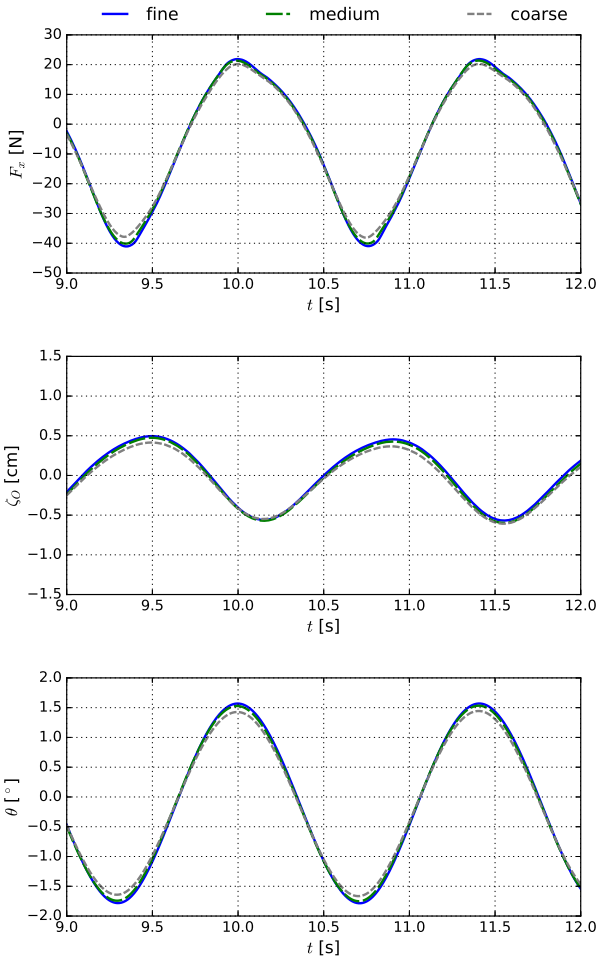


Figure 14: Grid dependence of longitudinal force, heave and pitch motions.

To check the grid dependence of the solution, some cases have been computed on two additional grids. Figure 14 shows time traces of the longitudinal force, as well as of the heave and pitch motions for $\lambda' = 1.0$, $\alpha = 0^\circ$ and $\zeta' = 0.01$. The grey trace was obtained on a grid with 680.000 cells, the green trace with 2.15 million cells and the blue one on a grid with 5.5 million cells. As can be seen, the accuracy of the results on the medium grid would be

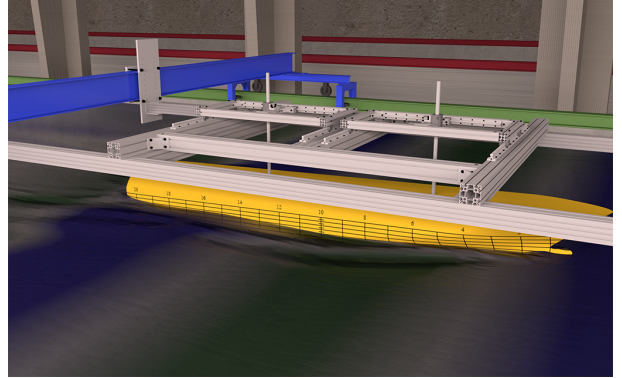


Figure 15: Implemented virtual spring system.

already sufficient for this relative long wave. However, since shorter wave lengths are also considered, all computations were carried out on the fine grid.

In the numerical simulations, the ship is completely free to heave and pitch, while roll is completely suppressed. The mean surge, sway and yaw motions are weakly prescribed using a virtual spring system. The system implemented resembles the one used in the towing tank of the Technical University Berlin and consists of two nested slides, which allow the motion in longitudinal and transverse direction, see Figure 15. Note that not only hydrodynamic forces but also the spring forces have to be considered at the right hand sides of the motion equations.

The computations were performed for 36 cases with non-dimensional wave lengths ranging from $\lambda' = 0.3$ to 1.0. The encounter angle has been varied from head to following waves in steps of 22.5° . Especially following waves are hard to generate with a field method due to the long time they need to develop and propagate into the domain when generated just at the boundaries. To improve this,

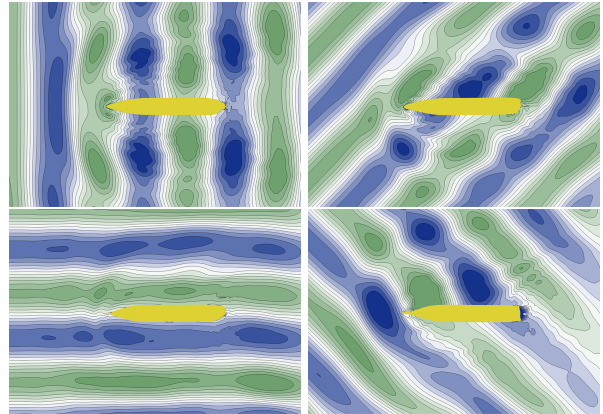


Figure 16: Snapshots of free surface elevation for waves from different directions with $\lambda' = 0.75$.

proper source terms have been added to the RANS equations in a certain region surrounding the ship. Figure 16 shows the free surface elevation for the computations with $\lambda' = 0.75$, $\zeta' = 0.0075$ and four different wave directions. The generated waves show the desired features.

The computations are performed using 500 time steps per wave period and 10 SIMPLE iterations on a single core. The computation time is approximately 70 hrs per period on the grid with 5.5 million cells. This small time step has been chosen to ensure an appropriate quality of the wave even for the shortest considered wave length of $\lambda' = 0.3$. Since the averaged forces are very small compared to the first order forces (see Figure 17) and can be influenced by very small reflections with high period as well as by motions at the natural frequency of the whole system, several wave periods are needed for accuracy.

Figure 17 shows the computed longitudinal and side force and the yaw moment acting on the ship for an incoming wave with a non-dimensional

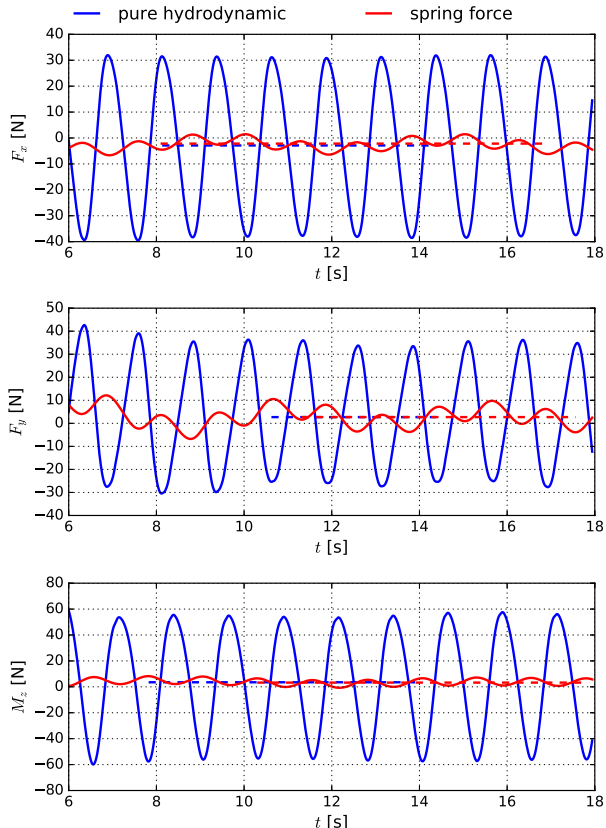


Figure 17: Longitudinal and side force and yaw moment (dashed lines show averages).

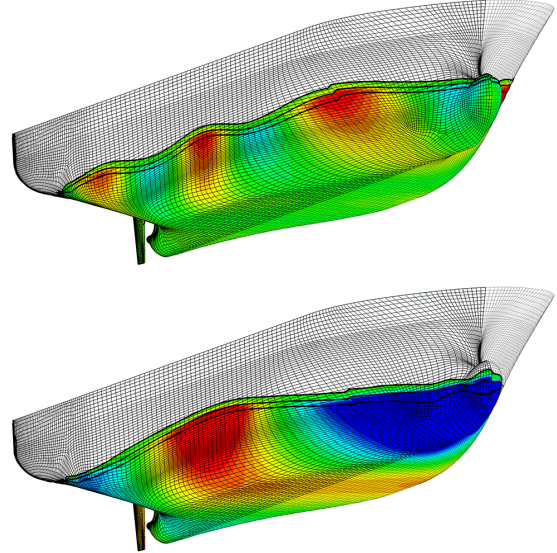


Figure 18: Free surface elevation and pressure distribution for two head waves.

wave length of $\lambda' = 0.75$, coming from $\alpha = 45^\circ$ with a non-dimensional amplitude of $\zeta' = 0.0075$. The two traces shown are the pure hydrodynamic force in the hybrid coordinate system, resulting from the integration of pressure and shear stresses on the surface of the ship, and the (negative) spring force. The difference between the two traces is due to inertial terms. The average of these terms is zero for the side force and yaw moment in this case (no roll), but (even if hardly visible) has a significant influence on the mean value of F_x due to heave and pitch. Since these terms have been disregarded in Equation 1 they are now included in the mean forces. Note that some hardly damped low frequency oscillations in the natural frequency of the whole system are superposed to the wave excited oscillations, especially in F_y .

In Figure 18 the computed pressure distribution and free surface elevation is qualitatively shown for two different head waves. The picture on the top shows a rather short wave with $\lambda' = 0.3$ and $\zeta' = 0.004$. The dynamic pressure on the hull is mainly due to the wave. The figure below shows a longer wave with $\lambda' = 0.75$ and $\zeta' = 0.0075$. In this case the dynamic pressure is not only due to the wave, but also strongly influenced by a positive pitch motion (bow upwards), which leads to a very high negative pressure at the bow.

The three lines between underwater hull and topsides in Figure 18 are contour levels of the signed distance function Φ used to separate the two phases of the fluid, water and air.

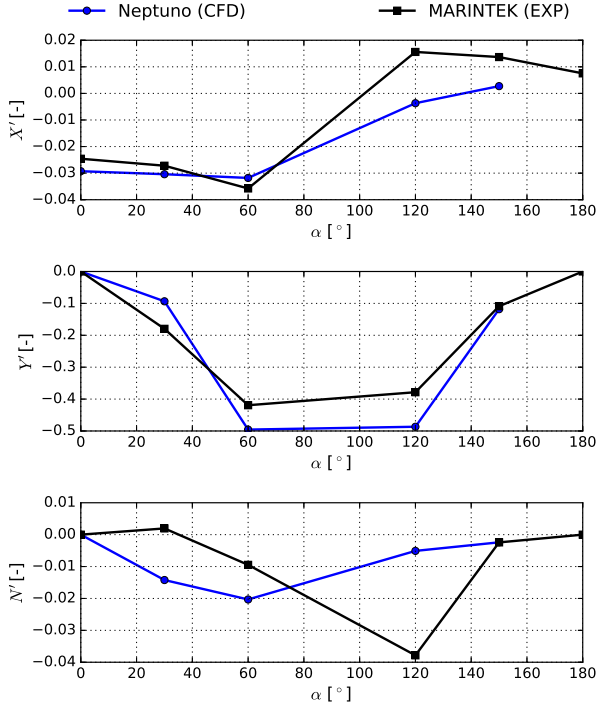


Figure 19: Computed mean forces for wave length $\lambda' = 0.28$ compared with measurements.

The middle line is the position of the free surface at the value $\Phi = 0$. For the stability of the numerical method a smooth transition of the density and viscosity between the two phases is needed. Therefore a thin region has been defined, where density and viscosity are interpolated between both fluids, indicated by the two other lines. To prevent this interpolation region from spreading, it is necessary to reinitialize the function Φ , Cura Hochbaum and Vogt (2002). As can be seen the interface could be kept quite sharp during the computations.

To validate the computed mean forces, additional computations have been performed for conditions tested at MARINTEK with $\lambda' = 0.2815$ and $\zeta' = 0.01056$. The results are shown in Figure 19. As can be seen, the agreement of the non-dimensional longitudinal and side force with the measurements is acceptable. The difference observed in the yaw moment could not be explained yet. In our opinion, the fact that the virtual test setup does not completely agree with the real tests does not explain this. Thus, further research is needed to check the accuracy of both, numerical and experimental results for such short, steep waves.

The comparison of computed and measured time traces for a wave with $\alpha = 30^\circ$ and $\lambda' = 0.28$

shows a very similar motion behaviour, see Figure 20. It should be noted that unfortunately, the measurements have been shifted, so that the mean values of the motions became zero. This was not done for the numerical results, thus especially the heave motion shows an offset mainly caused by dynamic sinkage.

After all the mean forces are computed, the coefficients of the mathematical model can be calculated. Symbols in Figure 21 show the results of the performed computations for nine encounter angles (α) and four non-dimensional wave lengths (λ').

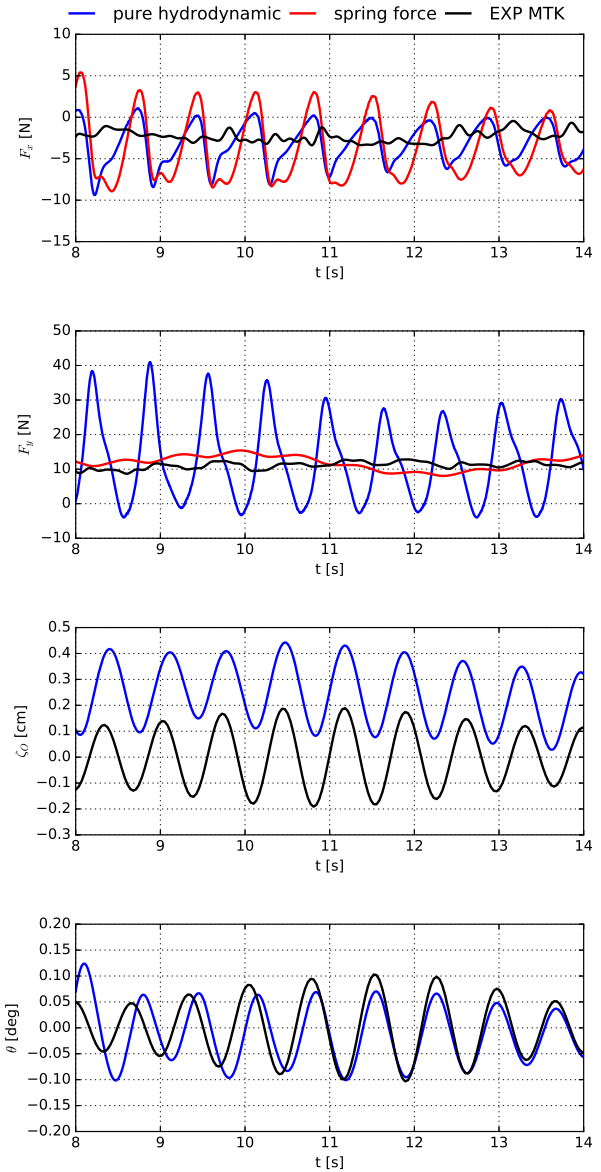


Figure 20: Computed time traces for $\alpha = 30^\circ$ and $\lambda' = 0.28$ compared with measurements.

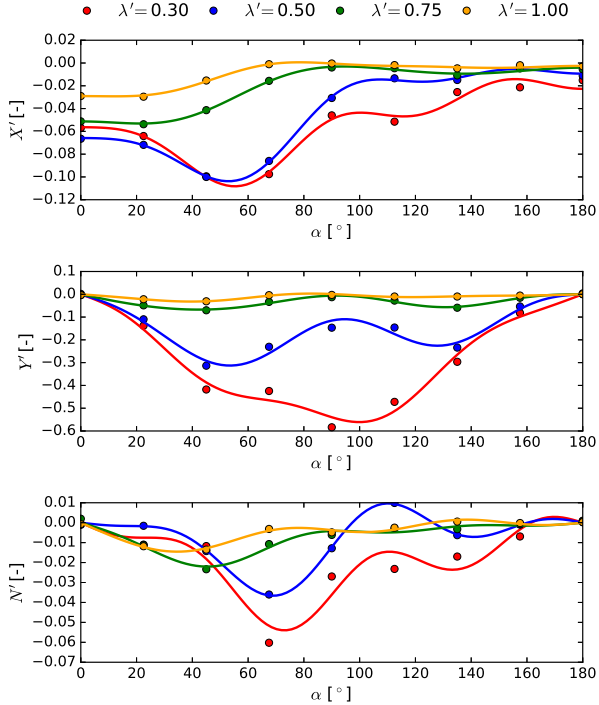


Figure 21: Computed mean forces in waves (symbols) and reconstructions (lines).

The lines in Figure 21 are the modelled forces, using only the coefficients a_{ni} and b_{ni} from the mathematical model. As can be seen, the model is able to capture well the computed values.

Figure 22 shows qualitatively the result of the mathematical model computed for wave lengths between 0.25 and 1.0 (radial direction) and all encounter angles. It can be seen that the maximum added resistance does not occur for the head wave condition, but in quartering head seas. This fact was already shown by other authors and confirmed during model tests at HSVA, Valanto and Hong (2015).

The maximum side force in short waves is found at beam seas as expected. However, for increasing wave length, it shifts towards head and following quartering seas. The side force in beam seas becomes almost zero. The yaw moment does not show such clear trends, but also has its maximum at head quartering seas.

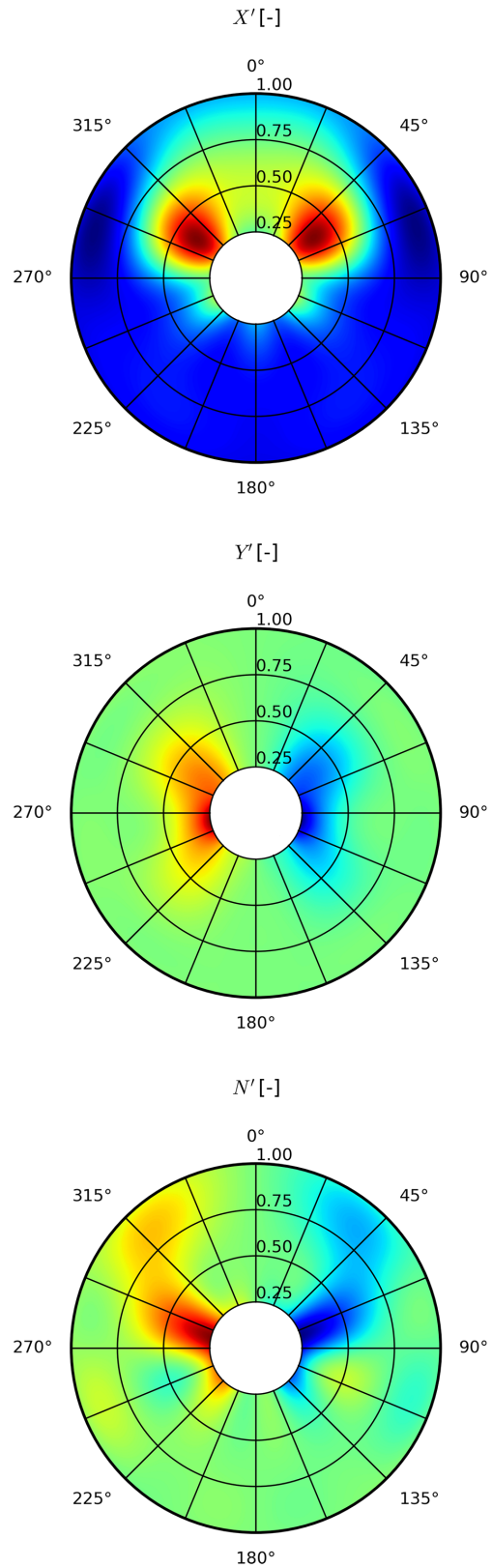


Figure 22: Modelled mean forces for different wave lengths and encounter angles.

MANOEUVRES IN WAVES

After all hydrodynamic coefficients of the expanded mathematical model are determined, any rudder manoeuvre in a regular wave of given length, earth-fixed direction and amplitude can be predicted with negligible computational time. Note that, although not shown here for simplicity reasons and not validated yet, it is basically possible to consider irregular waves, even short crested, using the present procedure. For this purpose, the mean wave forces and moments from the individual wave components of the seaway are calculated using the respective non-dimensional coefficients, multiplied by the squared wave amplitude according to the given spectrum.

Turning circle tests with 35° rudder deflection to starboard in regular waves of non-dimensional length $\lambda' = 0.686$ and amplitude $\zeta' = 0.00282$ have been predicted for the DTC with an approach speed of 6kn and compared with model tests from MARINTEK, Spenger et al. (2016). While the model was provided with simplified segmented bilge keels, they were not considered during the simulations. In addition, different to the model tests, where the (constant) propeller revolution has been adapted for each case to ensure the given mean approach speed, all simulations have been performed with a single hydrodynamic coefficient set, obtained with a propeller revolution roughly corresponding to the one needed in head waves. Thus, the propeller loading and the rudder inflow did not completely coincide with the experiments. To ensure the balance of thrust and resistance in waves, the total longitudinal force was zeroed at the beginning of each simulation.

Figure 23 shows the trajectories during turning circle tests starting at three different initial encounter angles, i.e. against, along and with the waves. As reported by other authors already, e.g. Ueno et al. (2003), Yasukawa and Nakayama (2009) and Seo and Kim (2011), the turning circles are not just shifted by the mean effect of the waves, but have also a significant twist relative to the earth-fixed direction of the incoming wave. The agreement of the computed results with the experiments is quite satisfactory. Both the shift and the twist are predicted acceptably well. The twist angle, being about 20° in clockwise sense in the present case, does not depend on the initial encounter angle but mainly on the wave length, see below.

The times t_{90} and t_{180} taken for the ship model to reach a heading change of 90° and 180° de-

pend on how the turning circle test starts as shown in Table 3. All predicted times are in satisfactory agreement with the experiments, the largest relative errors being about 10%. Especially the measured times t_{90} and t_{180} considerably increase compared to head waves when starting the manoeuvre along to the waves (turning into the waves) and when starting in following waves. This may be due to the fact that the propeller rate has been adapted according to the added resistance at the starting condition.

The relevance of Table 3 for judging manoeuvrability in waves is thus questionable. It would probably give more insight to perform all tests at the propeller revolution needed for keeping a required certain forward speed in the worst condition, independent of the resulting approach speed. There is no standard definition for manoeuvring tests in waves yet, and performing turning circles may not represent the best option in full scale, even if they yield very useful information for validation purposes.

Table 3: Times during turning circle tests

approach situation		SIM	EXP	DIFF
head	t_{90}	50 s	46 s	+9%
	t_{180}	96 s	94 s	+3%
beam	t_{90}	54 s	52 s	+5%
	t_{180}	105 s	103 s	+2%
following	t_{90}	52 s	53 s	-3%
	t_{180}	107 s	120 s	-11%

The time traces of the computed non-dimensional forward speed and drift angle during the turning circle tests mentioned above are compared with measurements with the DTC model in Figure 24. The agreement with low pass filtered experimental results is again very encouraging. Broadly speaking, the speed loss of about 60% and the mean drift angle of about 20° are predicted well. Note that, contrary to the computed traces, the unfiltered experimental time histories show the oscillations due to first order wave forces. The first part of the turning circle test starting against the waves has been enlarged and the corresponding heading angles have been added in Figure 25. The encounter frequency is always high enough and its variation during the manoeuvre, depending on the encounter angle and speed, is relatively small, as has been assumed for the validity of our procedure in the introduction.

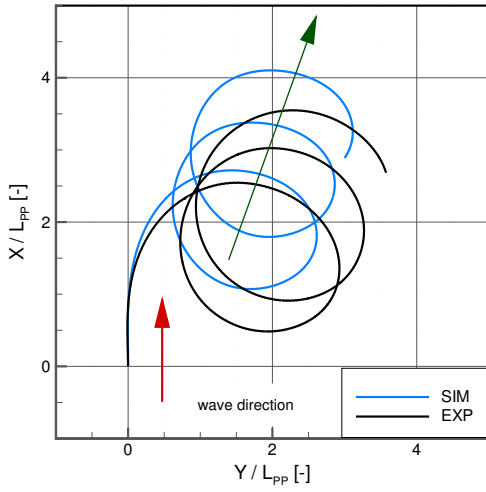
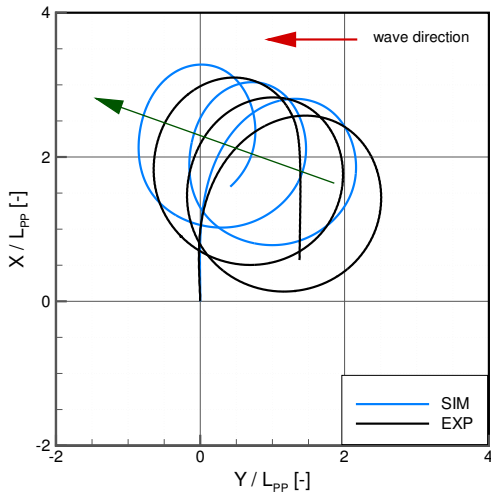
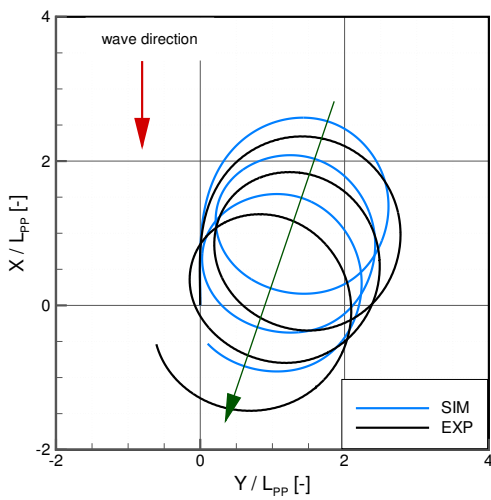


Figure 23: Simulated and measured turning circles for three different earth-fixed wave directions.

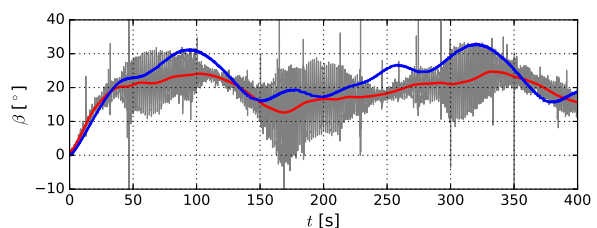
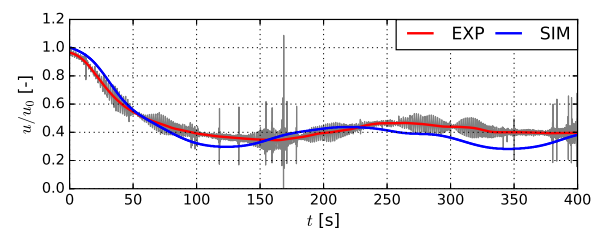
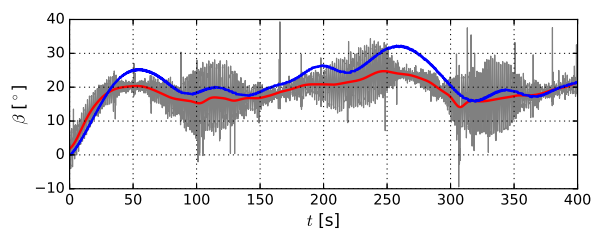
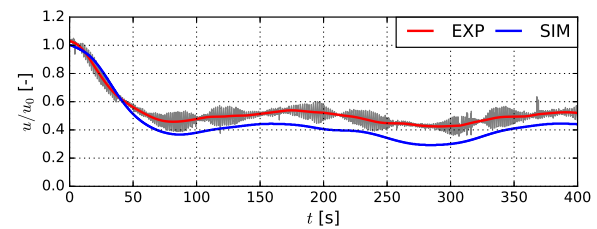
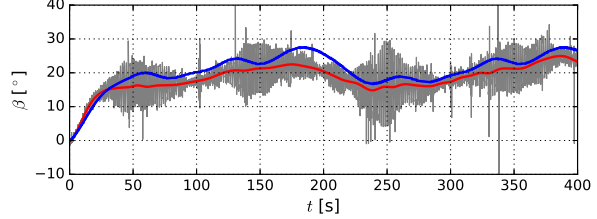
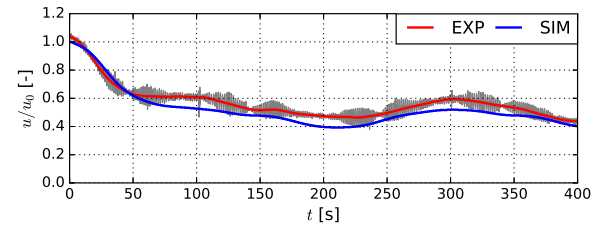


Figure 24: Simulated and measured time traces of forward speed and drift angle during turning circles.

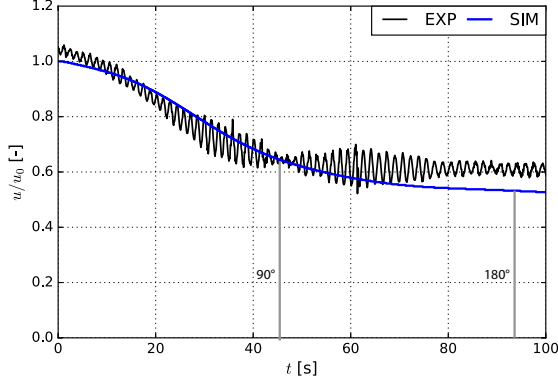


Figure 25: Zoomed time traces of forward speed and corresponding heading angles.

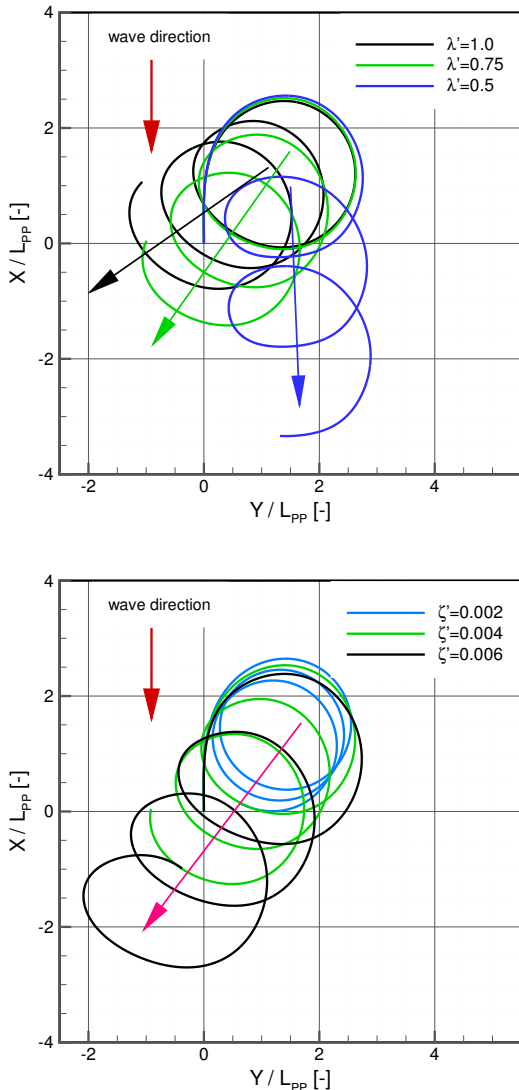


Figure 26: Simulated turning circles in waves of different lengths (top) and amplitudes (bottom).

The following additional simulated manoeuvres shed more light on the dependence of the turning circle test on the wave length and wave height. All tests have been performed with a rudder deflection of 35° to starbord. The diagram on the top of Figure 26 shows the influence of the wave length on the twist angle. For the three wave lengths considered, $\lambda'/L_{pp} = 1.0, 0.75$ and 0.5 , the height has been adapted to keep a constant wave steepness. As can clearly be seen, the (clockwise) twist of the turning circles displacement regarding the wave direction strongly increases with the wave length. It is also interesting to note that the shift of the turning circles is larger for the shorter waves, even if they have smaller amplitudes due to the constant steepness. The diagram on the bottom shows the dependence of the shift of the turning circles on the non-dimensional wave amplitude. The shift considerably increases with the amplitude, while the twist angle remains almost unchanged.

EQUILIBRIUM IN WAVES

A subset of the hydrodynamic coefficients for manoeuvring prediction can be used also for determining the required rudder angle and corresponding drift angle to ensure equilibrium under the mean effect of a regular wave of given length, direction and height. Such a 'mean' equilibrium situation, which disregards motions due to first order forces, would correspond to a ship sailing at a mean heading angle, forward and drift velocity. The analysis of the stability of such situations could give some insight into the course keeping ability of the ship in waves.

Assuming that the balance in longitudinal direction is ensured by the propeller thrust anyway, it is only necessary to iteratively solve the following equations in order to find the equilibrium situations:

$$\begin{aligned}
 & Y_v v_0 + Y_{vvv} v_0^3 + Y_\delta \delta_0 + Y_{\delta\delta\delta} \delta_0^3 + \\
 & + Y_{vv\delta} v_0^2 \delta_0 + Y_{v\delta\delta} v_0 \delta^2 + Y'_W(\alpha) \rho g \zeta_w^2 L_{pp} = 0 \\
 & N_v v_0 + N_{vvv} v_0^3 + N_\delta \delta_0 + N_{\delta\delta\delta} \delta_0^3 + \\
 & + N_{vv\delta} v_0^2 \delta_0 + N_{v\delta\delta} v_0 \delta^2 + N'_W(\alpha) \rho g \zeta_w^2 L_{pp}^2 = 0
 \end{aligned} \tag{4}$$

The needed rudder angle and the resulting mean drift velocity have been denoted with δ_0 and v_0 . Equation 4 contains all linear and non-linear hydrodynamic coefficients of the side force and yaw moment depending on the the drift velocity and rudder angle, indicated with indices v and δ . The mean wave side force and moment for the encounter angle α ,

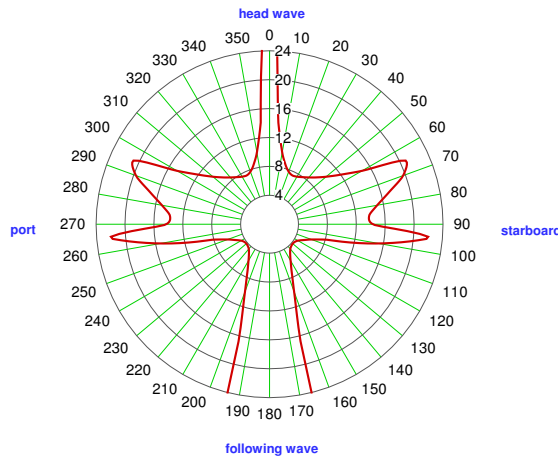


Figure 27: Maximum possible wave height in waves of length $\lambda' = 0.687$ from any direction.

according to Equation 3, have been denoted with $Y'_W(\alpha)$ and $N'_W(\alpha)$. For each wave length and encounter angle, it may be interesting to determine up to which wave amplitude or height can be sustained with rudder angles $\delta \leq 20^\circ$ for instance. This is shown in Figure 27 for the DTC sailing at 6 kn in waves of length $\lambda' = 0.687$. In this polar diagram, the encounter angle has been depicted in circumferential and the wave height in radial direction. The smallest allowed maximum wave height is roughly $H_w = 4$ m for $\alpha \approx 130^\circ$.

CONCLUSIONS

A new method for predicting rudder manoeuvres in waves, based on RANS simulations of captive model tests and taking into account mean wave forces and moments, has shown to yield very promising results for turning circle tests of a single screw ship. Important features observed in experiments, such as the shift of repeated turning circles by the mean effect of the waves and the twist with respect to the earth-fixed wave direction, are captured well. The twist mainly depends on the wave length, while the shift increases for shorter and higher waves.

Once the complete set of hydrodynamic coefficients has been determined, any manoeuvre can be simulated in negligible computational time. With minor changes, the method could also be used to predict manoeuvres in a seaway. Moreover, a subset of the hydrodynamic coefficients allows for determining the rudder and drift angle to achieve mean equilibrium in waves of given length, height and direction.

In order to judge the capabilities and the accuracy of the described procedure more thoroughly, further analysis and especially detailed experiments for validation purposes are indispensable.

ACKNOWLEDGEMENTS

This work has been supported by the German Ministry of Economic Affairs and Energy and the European Commission through the projects PerSee and SHOPERA, respectively. The authors also thank MARINTEK for providing the measurements as well as Mr. Lars Koopmann and Mr. Antonio Lengwinat for performing the RANS calculations for comparison of selected forces and for the body force database.

REFERENCES

- Cura Hochbaum A. and Vogt M. "Towards the simulation of seakeeping and maneuvering based on the computation of the free surface viscous ship flow". Proceedings of the 24th ONR Symposium on Naval Hydrodynamics, Fukuoka, Japan, 2002.
- Cura Hochbaum A. "Virtual PMM tests for manoeuvring prediction". Proceedings of the 26th ONR Symposium on Naval Hydrodynamics, Rome, Italy, 2006.
- Cura Hochbaum A., Vogt M., and Gatchell S. "Maneuvering prediction for two tankers based on RANS simulations". Proceedings of SIMMAN Workshop, Copenhagen, Denmark, 2008, p. F22.
- Cura Hochbaum A. and Uharek S. "Prediction of the manoeuvring behaviour of the KCS based on virtual captive tests". Proceedings of SIMMAN Workshop, Copenhagen, Denmark, 2014.
- Cura Hochbaum A., Koopmann L., and Yao J. "A body force model for approximating the propeller effect during RANS simulations for manoeuvring prediction". to appear, 2017.
- Faltinsen O.M. Sea Loads on Ships and Offshore Structures. Cambridge University Press, 1990.
- Osher S. and Sethian J.A. "Fronts Propagating with Curvature-Dependent Speed: Algorithms Based on Hamilton-Jacobi Formulations". Journal of Computational Physics, Vol. 79, (1988), pp. 12–49.

Patankar S.V. and Spalding D.B. "A Calculation Procedure for Heat, Mass and Momentum Transfer in Three-Dimensional Parabolic Flows". International Journal of Heat and Mass Transfer, Vol. 15, (1972), pp. 1787–1806.

Seo M.G. and Kim Y. "Numerical analysis on ship maneuvering coupled with ship motion in waves". Journal of Ocean Engineering, Vol. 38, (2011), pp. 1934–1945.

Spenger F., Hassani V., Maron A., Delefortrie G., van Zwijnsvoorde T., Cura Hochbaum A., and Lengwinat A. "Establishment of a validation and benchmark database for the assessment of ship operation in adverse conditions". Proceedings of the 35th International Conference on Ocean, Offshore Arctic Engineering, Busan, South Korea, 2016.

Sussman M., Smereka P., and Osher S. "A level set approach for computing solutions to incompressible two-phase flow". Journal of Computational Physics, Vol. 114, no. 1, (1994), pp. 146–159.

Ueno M., Nimura T., and Miyazaki H. "Experimental study on manoeuvring motion of a ship in waves". Proceedings of MARSIM, Tokyo, Japan, 2003.

Uharek S. and Cura-Hochbaum A. "Modelling Mean Forces and Moments Due to Waves Based on RANS Simulations". International Society of Offshore and Polar Engineers, Vol. 3, Kona, Hawaii, 2015, pp. 46–51.

Valanto P. and Hong Y. "Experimental Investigation on Ship Wave Added Resistance in Regular Head, Oblique, Beam, and Following Waves". International Society of Offshore and Polar Engineers, Vol. 3, Kona, Hawaii, 2015, pp. 19–26.

Wilcox D.C. Turbulence Modeling for CFD. 1st ed. DCW Industries, 1993.

Yao J. On the propeller effect when predicting hydrodynamic forces for manoeuvring using RANS simulations of captive model tests. dissertation, Technical University Berlin (2015).

Yasukawa H. and Nakayama Y. "6-DOF motion simulations of a turning ship in regular waves". Proceedings of MARSIM, Panama City, Panama, 2009.